INTELLIGENT SYSTEMS AND SUSTAINABLE ENERGY
E-ISSN: 3154-7532
VOLUME 1, ISSUE 2, 2026, page 80 - 95
DOI: https://doi.org/10.15282/isse.1.2.2026.15415

RESEARCH ARTICLE

Optimal reactive power dispatch using Smell Agent Optimization for transmission loss minimization considering multi-contingencies

Muhammad Izzuddin Salmizi[1], Nor Rul Hasma Abdullah[1*], Ibrahim Haruna Shanono[2] and Lailatul Niza Muhammad[1]

[1]Faculty of Electrical and Electronics Engineering Technology, Universiti Malaysia Pahang Al-Sultan Abdullah, 26600 Pekan, Pahang, Malaysia
[2]Electrical and Electronics Engineering Department, Bayero University Kano, Kano, Nigeria

Abstract – Optimal reactive power dispatch (ORPD) is a non-linear, non-continuous optimization problem that is central to secure and economic power system operation. This paper applies the Smell Agent Optimization (SAO) algorithm, a recently proposed nature-inspired metaheuristic based on the phenomenon of olfaction, to solve the ORPD problem while explicitly accounting for multi-contingency conditions. This appears to be one of the earliest applications of SAO to the ORPD problem under explicit multi-contingency conditions. The control variables optimized are generator terminal voltages, transformer tap ratios, and shunt capacitor sizes. The proposed approach is implemented and tested on the IEEE 30-bus reliability test system with 13 control variables using MATLAB R2017a and MATPOWER 5.1. Weak and secure buses are first identified through the Static Voltage Stability Index, and generator and line contingencies are ranked using the same index to select representative severe outages. A parametric study on the number of moles and iterations is conducted to establish a consistent SAO configuration (50 moles, 150 iterations), which is then used to minimize transmission loss under three scenarios: without outage, with a single line/generator outage (N-1), and with combined line-and-generator multi-contingency (N-2). At bus 26, SAO reduced transmission loss from 11.6957 MW to 6.9554 MW (40.5309%) at 25 MVAr loading without contingency, and from 13.9270 MW to 8.5120 MW under the combined multi-contingency case at the same loading, while the 13 control variables satisfied their equality and inequality constraints in every run; full post-optimization feasibility diagnostics are reported in Section 3.6. SAO reduces transmission loss consistently in every scenario tested, with and without contingencies, while every control variable stays within its operating limits.

Article history
Received : 2 August 2026
Revised : 3 September 2026
Accepted : 7 September 2026
Published : 21 September 2026

Keywords
Optimal reactive power dispatch
Smell Agent Optimization
Multi-contingency analysis
IEEE 30-bus system
Metaheuristic optimization

1. Introduction

Electrical power is generated, transmitted, distributed, and consumed continuously, and the delivery of adequate power to a constantly varying load is one of the central challenges faced by power system operators [1]. As power networks grow more complex, ensuring adequate voltage stability, power quality, security, and economic operation while accommodating load variation has become an increasingly demanding task for the power industry [2]. When abrupt disturbances such as contingencies occur, the system must still maintain voltage limits and active power flow restrictions while minimizing overall active power loss in the connected transmission lines. Reactive power must therefore be dispatched appropriately in both location and magnitude, making the optimal power flow (OPF) and optimal reactive power dispatch (ORPD) problems critical areas of research for reliable and economic power system operation [2]. Optimal power flow can be separated into real and reactive power dispatch sub-problems. The optimal reactive power dispatch (ORPD) problem is controlled through the generator voltage, transformer tap setting, and static VAR sources [3]. Traditional solution techniques, including quadratic, linear, non-linear, and interior-point programming [4], have gradually been replaced by modern population-based approaches such as genetic algorithms, particle swarm optimization, and differential evolution [5]. The amount of reactive power required varies with load and voltage level [6], and the resulting problem is non-linear with many local minima due to the mix of discrete devices (transformer taps, shunt capacitors) and continuous variables (generator voltages) [7]. Conventional optimization methods for ORPD suffer from convergence to local optima and rely on assumptions of convexity, differentiability, and continuity that do not hold for the real ORPD problem [7]. Metaheuristic optimization methods have therefore been widely adopted to overcome these limitations. Differential evolution has been used with modal analysis for ORPD [8], and a hybrid fuzzy-Jaya approach has been proposed to simultaneously reduce transmission loss and voltage deviation while satisfying equality and inequality constraints [9], [10]. Among swarm-based methods, particle swarm optimization (PSO) has been applied extensively to ORPD and reactive power loss minimization [11], [12], including a PSO-based ORPD formulation that explicitly considers multi-contingencies [13]. Moth-flame optimization (MFO), inspired by the navigation behaviour of moths toward light sources, has been used to minimize power loss and voltage

*CORRESPONDING AUTHOR | Nor Rul Hasma Abdullah | ✉ hasma@umpsa.edu.my

deviation on the IEEE 30-, 57-, and 118-bus systems [14]. The chaotic bat algorithm (CBA) has been applied to ORPD across multiple system sizes considering active loss, voltage deviation, and voltage stability index as objectives [15], while the crow search algorithm (CSA), inspired by the food-hiding behaviour of crows, has demonstrated competitive results for constrained engineering optimization problems including ORPD [16], [17], [18]. Hybrid approaches, such as the combination of artificial bee colony and salp swarm algorithms (ABC-SSA), have also been proposed to balance exploration and exploitation in solving the ORPD problem on IEEE-30 and IEEE-300 bus systems [19]. Other formulations include a modified genetic algorithm [20] and a charged system search algorithm [21] for ORPD. A separate line of work incorporates uncertainty from renewable generation and load directly into the ORPD formulation, for example, a marine predators algorithm [22], an adaptive Beluga whale optimizer [23], a modified artificial hummingbird algorithm [24], and an improved lightning attachment procedure optimizer [25]. Though these studies address load and renewable-generation uncertainty rather than discrete contingency events such as line or generator outages.

Across these studies, a common limitation is that multi-contingency handling is rarely treated explicitly: most report ORPD performance under a single operating condition or, at most, one contingency type, with limited statistical validation over repeated independent runs. The most directly comparable study is the PSO-based ORPD framework of [13], which considers multi-contingencies on the same IEEE 30-bus system; however, it is based on an older metaheuristic and does not combine SVSI-based weak-bus screening with Performance-Index outage ranking in the same integrated pipeline used here. The present study follows the same general contingency-analysis structure as [13] but substitutes SAO as the optimization engine. The Smell Agent Optimization (SAO) algorithm is a more recently introduced nature-inspired metaheuristic, first conceptualized as a feasibility study on smell-based agent navigation [26] and subsequently formalized as the Smell Detection Agent Optimization (SDAO) framework tested on CEC benchmark functions and a hybrid renewable energy system application [27]. SAO simulates the way biological agents perceive and trail scent molecules to locate a source, using three behavioural modes: sniffing, trailing, and random [28]. Despite its demonstrated performance on general optimization benchmarks, SAO has not been widely explored for power system applications such as ORPD, and in particular its behaviour under multi-contingency conditions, where both line and generator outages occur together, has not been reported in the literature. The closest related work is a PSO-based ORPD study that considers multi-contingencies on the IEEE 30-bus system [13]; we extend that same multi-contingency analysis framework (weak-bus identification via SVSI, outage ranking, and N-1/N-2 scenario evaluation) using SAO as the optimization engine. In summary, while metaheuristic ORPD solutions are well established for single-outage or outage-free conditions, there remains limited understanding of how a newer algorithm such as SAO performs when a network must simultaneously withstand combined line-and-generator outages. Addressing this gap requires an integrated framework that identifies weak buses, ranks credible contingencies, and evaluates loss-minimization performance for SAO under progressively more severe operating conditions, which is the problem this study addresses. The novelty of this study lies in applying SAO, among the first such applications, to the ORPD problem under explicit multi-contingency conditions on the IEEE 30-bus system, extending the PSO-based multi-contingency framework of [13] to a different, more recently proposed metaheuristic. The objectives of this study are: (a) to minimize the total power transmission loss in the power system by finding the best combination of the optimal setting for the control variables while considering multi-contingencies, and (b) to apply Smell Agent Optimization (SAO) to optimize the transmission loss considering multi-contingencies of the power system while satisfying equality and inequality constraints. The remainder of this paper is organized as follows: Section 2.1 presents the mathematical formulation of the ORPD problem; Section 2.2 describes the IEEE 30-bus test system, weak-bus identification, and contingency ranking procedure; Section 2.3 presents the SAO algorithm; Section 3 reports and discusses the results; and Section 4 concludes the paper.

2. Method and Materials

2.1. Problem formulation of ORPD

The ORPD problem is a sub-problem of OPF in which all control variables associated with reactive power which is generator output voltage, transformer tap ratio, and shunt reactor/capacitor output are determined [3]. OPF itself dates to the 1950s, when it was introduced as an extension of the classical economic dispatch problem. It captures the same idea of finding the best operating configuration for a power system, but under a fuller set of technical and security restrictions [1]. Economic dispatch minimizes generation cost alone, over a simplified network. OPF, and ORPD with it, keeps that cost objective but also enforces the full power-flow equations and operating limits of the network, which is exactly what makes the problem non-linear and, in general, non-convex. The general OPF/ORPD optimization problem is expressed as

$$\text{Minimize} \quad f(x,u) \tag{1}$$

subject to

$$g(x,u) = 0, \qquad h(x,u) \leq 0 \tag{2}$$

where f is the objective function representing transmission line losses, $g(x,u) = 0$ expresses the equality constraints for the real and reactive power flow equations of the network, and $h(x,u) \leq 0$ expresses the inequality constraints for power flow and other security restrictions. Here x and u denote the vectors of dependent and control variables, respectively.

2.1.1. Objective function

The objective is to minimize the total real power loss in the transmission lines while satisfying all operational constraints [11]:

$$P_{loss} = \sum_{k=(i,j)}^{k=N_E} g_k \left(V_i^2 + V_j^2 - 2V_iV_j\cos(\theta_i - \theta_j)\right) \tag{3}$$

where N_E is the set of all branches and g_k is the conductance of branch k. Since the bus voltages are implicit functions of the control variables, the power loss is a non-linear function of those variables.

2.1.2. Equality constraints

The equality constraints represent the real and reactive power balance at each bus [3]:

$$P_{Gi} - P_{Di} = V_i \sum_{j\in N_i} V_j \left(G_{ij}\cos\theta_{ij} + B_{ij}\sin\theta_{ij}\right) \tag{4}$$

$$Q_{Gi} - Q_{Di} = V_i \sum_{j\in N_i} V_j \left(B_{ij}\cos\theta_{ij} - G_{ij}\sin\theta_{ij}\right) \tag{5}$$

where V_i and V_j are the voltages at bus i and bus j, B_{ij} and G_{ij} are the susceptance and conductance between bus i and bus j, P_{Gi} and Q_{Gi} are the real and reactive power generation, and P_{Di} and Q_{Di} are the real and reactive load demand, respectively.

2.1.3. Inequality constraints

The inequality constraints include the operational limits of generators, transformers, and reactive compensation devices [3]. Discrete variables such as transformer taps and shunt capacitors are treated as continuous during the search itself, which is standard practice in metaheuristic ORPD formulations; enforcing discreteness directly would substantially complicate the optimizer for little practical gain. Once the search converges, the continuous values are converted back to their nearest practical setting and rounded to four decimal places. The generator real power, reactive power, and voltage limits are

$$P_{Gi}^{min} \le P_{Gi} \le P_{Gi}^{max} \tag{6}$$

$$Q_{Gi}^{min} \le Q_{Gi} \le Q_{Gi}^{max} \tag{7}$$

$$V_{Gi}^{min} \le V_{Gi} \le V_{Gi}^{max} \tag{8}$$

for $i = 1, \dots, N_G$, where N_G is the number of generators. The transformer tap ratio is constrained by

$$T_{Gi}^{min} \le T_{Gi} \le T_{Gi}^{max} \tag{9}$$

for $i = 1, \dots, N_T$, where N_T is the number of transformers, and the reactive compensator sizing is constrained by

$$Q_{Ci}^{min} \le Q_{Ci} \le Q_{Ci}^{max} \tag{10}$$

for $i = 1, \dots, N_C$, where N_C is the number of reactive compensators.

In this implementation, the box constraints on the 13 control variables (Eqs. 8-10) are enforced directly by the optimizer: any candidate value that falls outside its Table 1 bound is clipped back to that bound after every position update (Section 2.3). The generator reactive-power limit (Eq. 7), together with bus voltage limits at load buses and branch thermal loading, is not enforced as an explicit penalty term inside the objective function; the objective (Eq. 3) is computed directly from the AC power-flow solution at each candidate solution, with no penalty added for constraint violation elsewhere in the network. Feasibility with respect to these remaining limits, and to load-flow convergence itself, is instead verified after optimization by re-solving the power flow at the reported solution and checking every bus voltage, generator reactive output, and branch loading against its operating limit; a run in which the load flow fails to converge is treated as infeasible. This post-optimization feasibility check is reported together with best/mean/median/standard-deviation/worst loss over 30 independent runs of the fixed SAO configuration in Section 3.6: every run converged and respected the control-variable bounds, but none passed the full feasibility check, with modest but systematic bus-voltage and generator reactive-power violations (Table 15).

2.2. IEEE 30-bus test system and contingency analysis

2.2.1. IEEE 30-bus reliability test system

The proposed approach is tested on the IEEE 30-bus RTS with 13 control variables: the voltage magnitudes of six generators at buses 1, 2, 5, 8, 11, and 13; four discrete transformer tap ratios on branches 6-9, 6-10, 4-12, and 27-28; and three discrete shunt VAR compensators at buses 3, 10, and 24 [14]. The system also has 24 PQ (load) buses and 41 transmission lines. All load-flow computations were performed in MATLAB R2017a using MATPOWER 5.1, an open-source power-system simulation package, with the system base at 100 MVA. The case data (bus, branch, and generator parameters) is the standard IEEE 30-bus RTS as distributed with MATPOWER, unmodified; the 13 control variables in Table 1 are existing generator, transformer, and shunt-compensator elements of that case treated as decision variables, not new network elements, and branch power flows follow MATPOWER's standard from-bus/to-bus convention throughout. SAO was implemented as a wrapper around MATPOWER's AC power-flow solver, so every candidate control-variable setting generated during the search is checked against a full AC load-flow solution, not a linearized approximation. The IEEE 30-bus RTS was chosen for a practical reason: it is a standard benchmark already reported widely in the ORPD literature, which means the transmission-loss results here can be read against the same system configuration used in related studies [11], [14]. The single-line diagram of the test system is shown in Figure 1. To satisfy the equality and inequality constraints, the boundary setting for each control variable is fixed at approximately ±10%, as summarized in Table 1.

2.2.2. Weak and secure bus identification

Five load buses which 14, 25, 26, 29, and 30 were selected to identify the weakest and most secure buses in the IEEE 30-bus RTS, reusing the same five candidate buses identified by prior screening of the full set of load buses in [13], rather than re-screening all 24 load buses for this study. The Static Voltage Stability Index (SVSI) gauges how close a bus is to voltage collapse; it is evaluated at rising reactive-load levels at each candidate bus, and the maximum loadability point is recorded as the highest load at which SVSI can still be computed, just before the AC load flow stops converging (Table 2). A bus that diverges early, at a low reactive load, has little margin left before voltage instability and counts as weak. One that keeps converging under a much heavier load has more margin and counts as secure. SVSI is a line-based voltage stability index formulated for a general two-bus system, originally developed by Qi [30] and applied here for weak-bus identification and outage ranking following the same approach as [13]. For a line connecting sending-end bus i and receiving-end bus j with impedance $Z_{ji} = R_{ji} + \mathrm{j}X_{ji}$, carrying complex power $S_{ji} = P_{ji} + \mathrm{j}Q_{ji}$ at the receiving end, solving the resulting voltage quadratic equation for bus j yields the SVSI for line ji, given in equation (11):

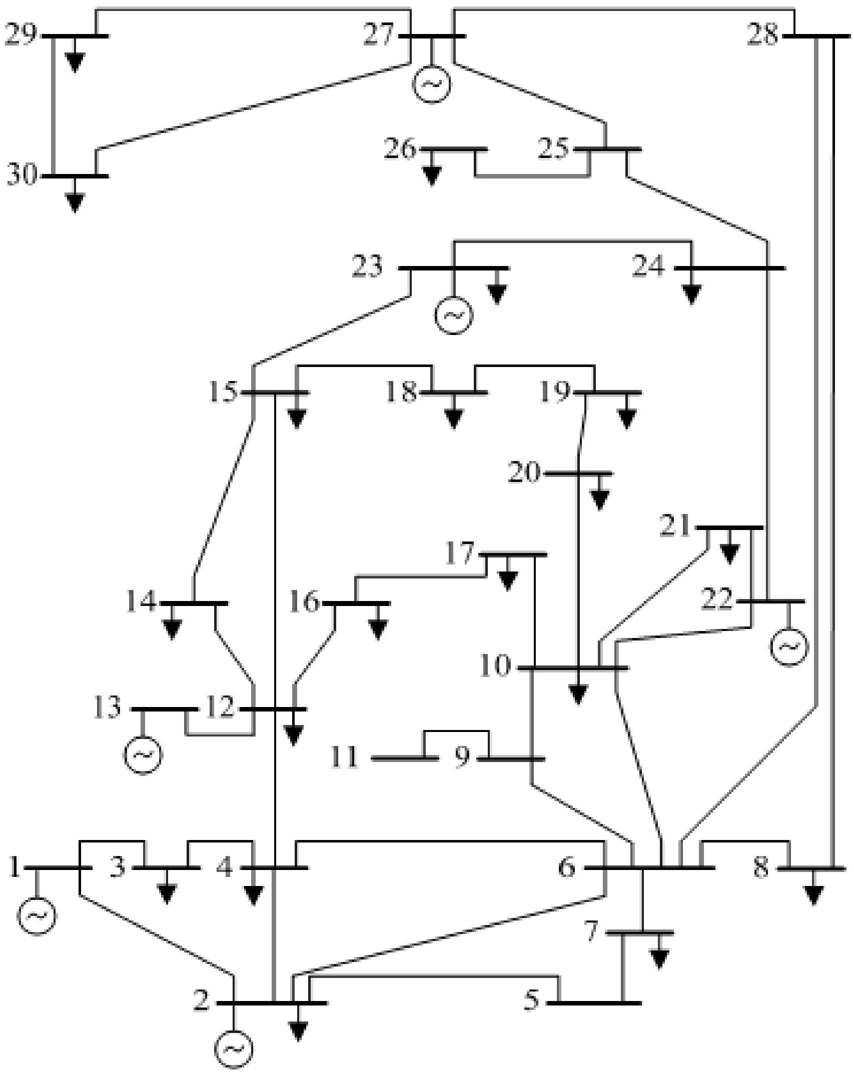

Figure 1. Single-line diagram of the IEEE 30-bus RTS [29]

Table 1. Upper and lower boundary setting of control variables [14]

Control variable	No. of variables	Lower bound	Upper bound
Generator voltage magnitudes, VG	6	0.9 p.u.	1.1 p.u.
Transformer tap ratios, T	4	0.95 p.u.	1.05 p.u.
Shunt reactive compensators, QC	3	−12 MVAr	36 MVAr
Total control variables	13	—	—

$$SVSI_{ji} = \frac{2\sqrt{({X_{ji}}^2 + {R_{ji}}^2)({P_{ji}}^2 + {Q_{ji}}^2)}}{|V_i|^2 - 2X_{ji}Q_{ji} - 2R_{ji}P_{ji}} \tag{11}$$

A value of SVSI approaching 1 indicates proximity to voltage collapse for that line, while lower values indicate a larger stability margin.

Bus 26 has the lowest maximum loadability and is therefore identified as the weakest bus, able to withstand a reactive loading of only 3.2 p.u. (approximately 32 MVAr) before voltage instability occurs [13]. Conversely, bus 14, with the highest maximum loadability, is identified as the safest bus, tolerating reactive loading of up to 70 MVAr. We accordingly selected bus 26 as the test bus for the loss-minimization case studies presented in Section 3. This 32 MVAr figure is a voltage-stability stress-test limit: it comes from progressively raising the reactive load at bus 26 alone, with no line or generator outage, until SVSI approaches its practical collapse threshold of about 0.9. It is therefore not the same quantity as the loading range swept in the ORPD case studies of Section 3 (Tables 7-13), which covers 0 to 25 MVAr at bus 26 under normal and contingency conditions alike; that range was kept within a practical operating margin below the 32 MVAr stress-test limit, rather than extended to the system's voltage-collapse boundary itself.

2.2.3. Contingency analysis

Contingency analysis examines how equipment outages, such as generators, transformers, and transmission lines, affect system stability [31]. A power grid is a network of interconnected machines, and one component failing during operation can compromise the whole system; power-system planning therefore tries to estimate the severity of every plausible outage ahead of time, rather than dealing with each one only after it happens [31]. Running a full AC load-flow analysis after every conceivable outage would be too slow to be practical, so contingencies are screened instead using a Performance Index, an intensity score for each outage case based on how badly it violates power-flow and voltage limits. Active-power violations and reactive-power/voltage violations are usually scored separately, as PIP and PIV, respectively. Ranking outages by this index shortlists the cases that actually matter and sets aside the ones posing negligible risk. For the IEEE 30-bus RTS, this meant evaluating 41 individual line-outage cases (one line at a time) by AC load-flow analysis and ranking them by Performance Index [13].

For generator outages, each of the six generators (excluding the slack bus at bus 1) was disconnected in turn, and the maximum SVSI recorded across all load variations was used to rank severity, as shown in Table 3. Generator 13 has the highest SVSI (0.1695p.u.), followed by generator 11 (0.1694p.u.); generator 13 was therefore selected as the representative severe generator outage for this study [13]. The same ranking procedure applied to the 41 line outages is summarized in Table 4 [13]. Line 1 has the highest SVSI (0.5008p.u.), but since bus 1 is the slack bus, line 9 (SVSI = 0.2436p.u.) was selected as the representative severe line outage.

For each loading and contingency scenario considered in this study - no outage, the line 9 outage, the generator 13 outage, and the combined multi-contingency case - the SAO algorithm is run independently to obtain a corrective dispatch: a fresh set of the 13 control-variable values, optimized specifically for that scenario's post-contingency network topology and loading level. This is not a single preventive setting required to remain feasible across every contingency simultaneously; it is why the optimized control variables reported in Tables 8, 11, and 13 differ from one another even though the underlying generator, transformer, and shunt-compensator buses are the same across scenarios.

2.3. Smell Agent Optimization (SAO) algorithm

Olfaction — the sense of smell — is one of the most fundamental ways living organisms detect chemical compounds in their environment, for finding food, mating, and avoiding danger [28]. Most biological agents rely on it for roughly the same purposes regardless of species, and that sniffing-trailing-searching behaviour turns out to be a useful template for

Table 2. Maximum reactive power loading of selected buses in the IEEE 30-bus RTS [13]

Bus	Maximum reactive power loading (p.u.)
14	7.0
25	7.0
26	3.2
29	3.7
30	3.5

Table 3. Generator outage ranking based on SVSI in the IEEE 30-bus RTS [13]

Rank	Generator outage no.	SVSI (p.u.)
1	13	0.1695
2	11	0.1694
3	2	0.1634
4	8	0.1611
5	5	0.1463

a population-based search procedure, much as flocking or predator-prey behaviour has inspired other nature-inspired metaheuristics before it. Salawudeen, Mu'azu, Sha'aban, and Adedokun built the Smell Agent Optimization (SAO) algorithm around exactly this relationship in 2021 [28], modelling an agent's interaction with its environment through three behavioural modes: sniffing, trailing, and random [26], [27].

SAO was selected for this study because it has demonstrated competitive performance against established metaheuristics on CEC benchmark functions [28], while requiring relatively few control parameters compared with algorithms that need additional coefficients to balance exploration and exploitation. Its three-mode search behaviour also gives it a natural mechanism for switching between broad exploration and local refinement, which motivated its application to the discrete-continuous, multi-modal ORPD search space.

2.3.1. Sniffing mode

In sniffing mode, a population of N smell molecules is initialized at random positions within a D-dimensional hyperspace, where D is the number of decision (control) variables (Figure 2). Each row of the resulting population matrix is one molecule; one candidate solution and each column is one of the D control variables being optimized. Whichever molecule has the highest fitness at a given stage of the search is, in effect, the best combination of generator voltages, transformer taps, and shunt-capacitor settings found so far.

The population of smell molecules is initialized as the matrix [28]

$$x_i^{(t)} = \left[x_{(n,d)}\right]_{N\times D}, \quad n = 1, \dots, N, \ d = 1, \dots, D \tag{12}$$

with each molecule's initial position generated using

$$x_i^{(t)} = lb_i + r_0 \times (ub_i - lb_i) \tag{13}$$

where ub_i and lb_i are the upper and lower bounds of the decision variables and r_0 is a random number in the range $(0,1)$. The corresponding initial velocity matrix is

$$v_i^{(t)} = \left[v_{(n,d)}\right]_{N\times D}, \quad n = 1, \dots, N, \ d = 1, \dots, D. \tag{14}$$

Table 4. Line outage ranking based on SVSI in the IEEE 30-bus RTS [13]

Rank	Line outage no.	SVSI (p.u.)
1	1	0.5008
2	9	0.2436
3	7	0.2120
4	6	0.1995
5	8	0.1977
6	2	0.1954
7	4	0.1946
8	5	0.1935
9	15	0.1877
10	11	0.1869

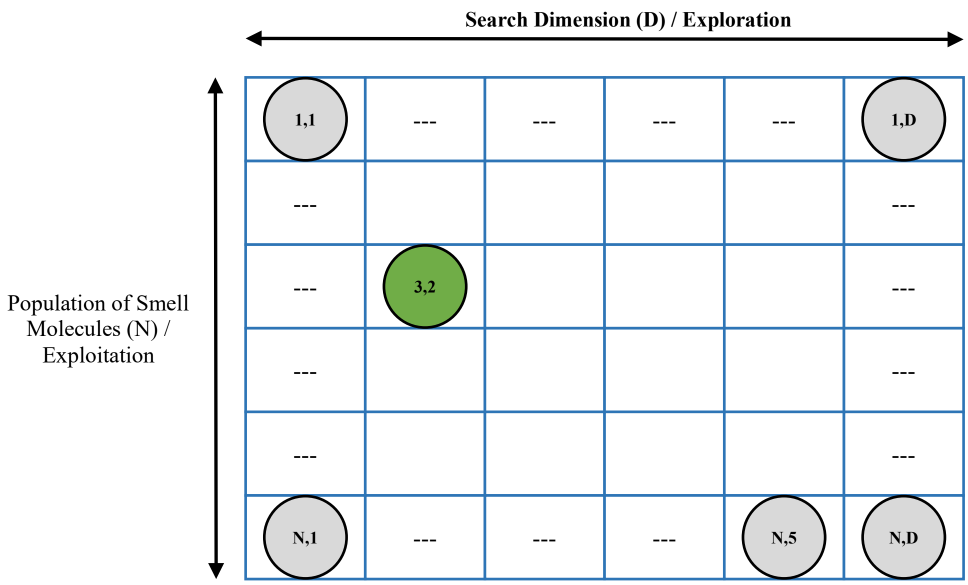

Figure 2. Smell position in hyperspace [28]

Since smell molecules follow Brownian motion, their positions and velocities are continuously updated as

$$x_i^{(t+1)} = x_i^{(t)} + v_i^{(t+1)} \times \Delta t \tag{15}$$

which, for a single optimization time-step ($t = 1$), simplifies to

$$x_i^{(t+1)} = x_i^{(t)} + v_i^{(t+1)} \tag{16}$$

and the velocity is updated using

$$v_i^{(t+1)} = v_i^{(t)} + \delta v \tag{17}$$

where the velocity increment δv is proportional to

$$\delta v = r_1 \times \sqrt{\frac{3kT}{m}} \tag{18}$$

with T and m representing the temperature and mass of the smell molecule and k normalizing the influence of temperature and mass on the kinetic energy of the molecule, based on the gas-pressure-difference analogy.

$$\frac{1}{2} nmv^2 = \frac{3}{2} knT \tag{19}$$

2.3.2. Trailing mode

Trailing mode models the agent's ability to follow the scent trail toward its source once a location of higher molecule concentration is detected, as illustrated conceptually in Figure 3. If the agent detects a location with a higher concentration of smell molecules while sniffing, it moves toward that location according to [28]

$$x_i^{(t+1)} = x_i^{(t)} + r_2 \times olf \times \left(x_{agent}^{(t)} - x_i^{(t)}\right) - r_3 \times olf \times \left(x_{worst}^{(t)} - x_i^{(t)}\right) \tag{20}$$

where $x_{agent}^{(t)}$ is the position of best fitness, $x_{worst}^{(t)}$ is the position of worst fitness, olf is the olfactory coefficient of the agent, and r_2, r_3 are random numbers in $(0,1)$.

2.3.3. Random mode

If the agent is unable to maintain the trail and becomes trapped in a local optimum, it transitions into random mode to continue exploring the search space [28]:

$$x_i^{(t+1)} = x_i^{(t)} + r_4 \times SL \tag{21}$$

where SL is a constant step length and r_4 is a random number that stochastically scales the step. Random mode prevents the agent from stagnating in a local optimum when the trailing mechanism loses the scent trail. The overall SAO procedure applied to the ORPD problem, including the handling of line and generator outage settings, is summarized in the flow chart in Figure 4.

3. Results and Discussion

All simulations were carried out in MATLAB R2017a using MATPOWER 5.1 to solve the AC load flow for the IEEE 30-bus RTS.

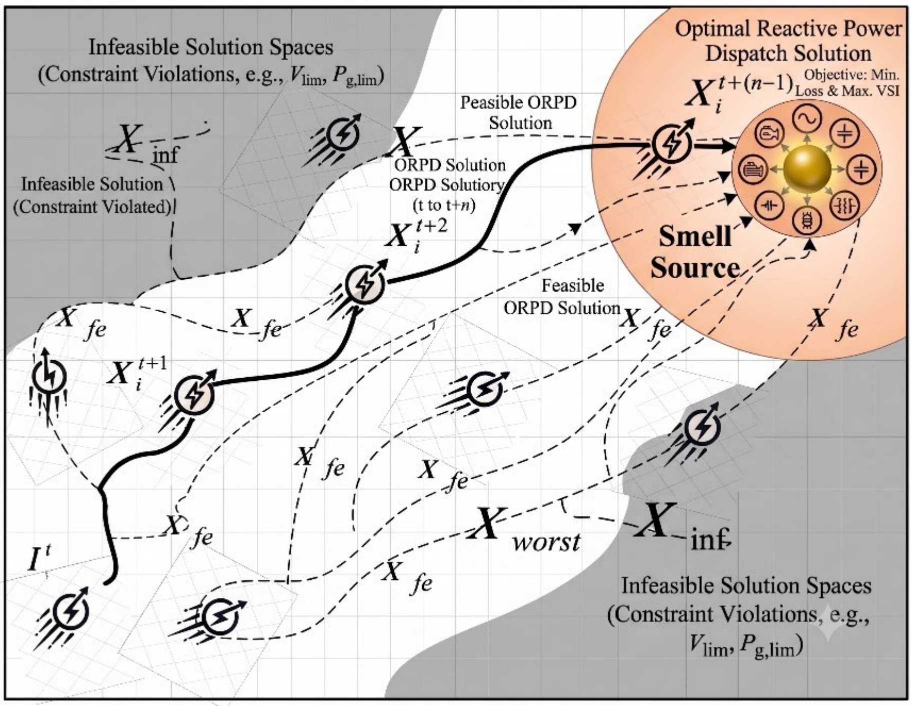

Figure 3. Conceptual framework of SAO for ORPD [28]

3.1. Preliminary result

The correlation between reactive loading and transmission loss was first examined at the previously identified weak bus (26) and secure bus (14), with and without contingency, as summarized in Tables 5 and 6. As expected, transmission loss increases with loading at both buses, and losses are consistently higher whenever a line or generator outage is present. Bus 26 tolerates a maximum load of only 25 MVAr (11.6960 MW without outage) before the system becomes unstable, confirming it as the weaker of the two buses, whereas bus 14 tolerates a maximum load of 70 MVAr (12.6400 MW without outage) sustains a considerably larger reactive load range without divergence [13]. Generator outages hurt more than line outages, and the gap widens as loading rises. At bus 14, the generator outage adds relatively little at light loading (6.6122 MW versus 5.6656 MW at 0 MVAr), but by 70 MVAr it pushes the loss to 28.6717 MW — more than double the no-outage value of 12.6400 MW. The line outage at line 9, by contrast, tracks the no-outage curve closely throughout (13.1341 MW at 70 MVAr). Bus 26 shows the same asymmetry at a much lower loading ceiling: the generator outage adds about 17% to the no-outage loss even at 0 MVAr (6.5706 MW versus 5.5950 MW), and the bus reaches its instability limit at just 25 MVAr, nowhere near the 70 MVAr bus 14 can sustain. That gap between the two outage types shows up earliest, and most sharply, at the weaker of the two buses.

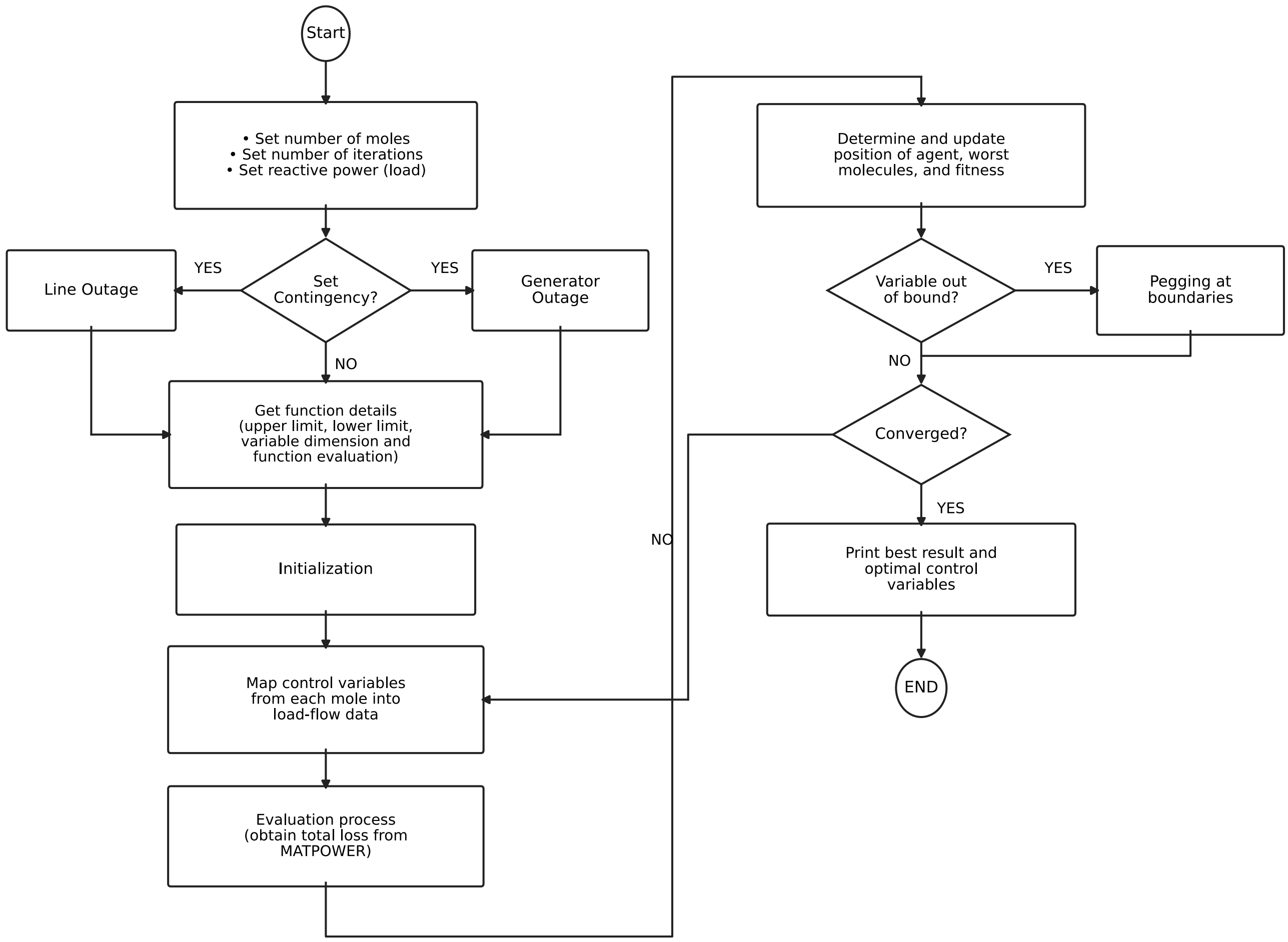

Figure 4. Smell Agent Optimization flow chart applied to the ORPD problem

Table 5. Active power loss with and without outage at bus 14

Loading QL (MVAr)	Without outage	Line outage at bus 9	Generator outage at 13
0	5.6656	6.2589	6.6122
10	5.7390	6.3275	6.8718
20	6.0367	6.6181	7.4859
30	6.5937	7.1655	8.5615
40	7.4558	8.0150	10.2768
50	8.6852	9.2281	12.9712
60	10.3696	10.8913	17.4835
70	12.6400	13.1341	28.6717

3.2. Case 1: Effect of number of moles and iterations

To establish a consistent SAO configuration for the subsequent case studies, the effect of population size (number of moles: 10, 20, 30, 40, 50) and number of iterations (50, 100, 150) on the transmission loss at bus 26 (0 MVAr loading) was evaluated, as shown in Table 7. The lowest transmission loss (4.8296 MW) is obtained with 50 moles and 150 iterations, well below the pre-ORPD losses of 5.6656 MW at bus 14 and 5.5950 MW at bus 26. More moles do not automatically mean a better result: 40 moles at 50 iterations gives 4.8839 MW, actually worse than the 4.8436 MW obtained with just 30 moles at the same 50 iterations. Population size and SAO's outcome on this problem are not monotonically related: 20 moles is the weakest population size tested, performing worse than even 10 moles, while the lowest overall loss comes from 50 moles at 150 iterations — more agents does not consistently help. What the whole table does show is a narrow spread: every combination tested falls between 4.8296 and 4.9306 MW, within about 2.1% of each other, regardless of how the moles and iterations are set. Table 8 lists the optimal control variable settings for the best configuration; under the further-corrected code, eight variables — V1, V2, V8, V11, V13, T6-10, T4-12, and T27-28 — sit at their upper bounds, while V5, T6-9, Qc3, Qc10, and Qc24 settle at interior values within the bounds defined in Table 1. Unlike the earlier (pre-fix) result, the three shunt compensators no longer cluster near 1.0 — Qc3, Qc10, and Qc24 now spread across 0.3701–10.2896 MVAr, consistent with their much wider −12 to 36 MVAr bound in Table 1. Since 50 moles at 150 iterations and 30 moles at 50 iterations produced the two lowest losses in the further-corrected Table 7 sweep, ten independent trials were run for each configuration to evaluate consistency, as shown in Table 9. Under the further-corrected SAO_FIXED2.m code, 50 moles at 150 iterations gives the lower average loss (4.8617 MW versus 4.8777 MW for 30 moles at 50 iterations), though not the tighter spread: its range of 4.8330–4.9067 MW (0.0737 MW) is wider than the 4.8383–4.8972 MW (0.0589 MW) seen at 30 moles and 50 iterations. The lower average carries more weight for choosing the fixed configuration, and it is also consistent with the lowest-loss combination already identified in the Table 7 sweep, so we adopt 50 moles and 150 iterations for the remaining case studies (Sections 3.3 and 3.4).

Table 6. Active power loss with and without outage at bus 26

Loading QL (MVAr)	Without outage	Line outage at bus 9	Generator outage at 13
0	5.5950	6.1910	6.5706
5	5.8130	6.4010	6.7800
10	6.3280	6.9050	7.3104
15	7.2590	7.8170	8.3051
20	8.8410	9.3670	10.0738
25	11.6960	12.1510	13.6496

Table 7. Transmission loss (MW) for varying number of moles and iterations

No. of moles	Iteration = 50	Iteration = 100	Iteration = 150
10	4.8919	4.9306	4.8660
20	4.8868	4.8860	4.9266
30	4.8436	4.8955	4.8894
40	4.8839	4.8932	4.8550
50	4.8796	4.8976	4.8296

Table 8. Optimal control variable values by SAO (50 moles, 150 iterations)

Variable	Optimal value
V1	1.1000 p.u.
V2	1.1000 p.u.
V5	1.0870 p.u.
V8	1.1000 p.u.
V11	1.1000 p.u.
V13	1.1000 p.u.
T6-9	1.0389 p.u.
T6-10	1.0500 p.u.
T4-12	1.0500 p.u.
T27-28	1.0500 p.u.
Qc3	0.8518 MVAr
Qc10	0.3701 MVAr
Qc24	10.2896 MVAr

3.3. Case 2: Reactive power variation without line outage and generator outage at bus 26

With the SAO configuration fixed at 50 moles and 150 iterations, the reactive loading at bus 26 was increased from 0 to 25 MVAr without any contingency to evaluate loss minimization performance, as shown in Table 10. At the maximum feasible loading of 25 MVAr, SAO reduced the transmission loss from 11.6957 MW to 6.9554 MW, a reduction of 40.5309%. That reduction is not fixed — it climbs at almost every step of the sweep, from 13.1336% at 0 MVAr up to 40.5309% at 25 MVAr. In practice, SAO does more work exactly where more work is needed: its advantage over the unoptimized system grows as the bus is pushed toward its loading limit, rather than staying flat regardless of stress. Table 11 lists the corresponding optimal control variables; V2, V5, and V13 sit at their lower bound of 0.9 p.u., T6-10 sits at its lower bound of 0.95 p.u., and T27-28 sits at its upper bound of 1.05 p.u. — a mix of both bound directions, rather than voltage support and tap ratios being pushed uniformly high, holds the loss down at this loading. The convergence behaviour of SAO for this scenario is shown in Figure 5. The algorithm reaches its final solution within 32 iterations, out of the 150 allowed per run — most of the iteration budget simply goes unused. That speed comes from how SAO searches: alternating between sniffing, trailing, and random modes (Section 2.3) lets it home in on a promising region early and spend the rest of the run refining rather than exploring from scratch.

3.4. Case 3: Reactive power variation with line outage, generator outage, and multi-contingency at bus 26

The same reactive loading sweep (0–25 MVAr) at bus 26 was repeated under three contingency conditions: a single line outage at line 9, a single generator outage at generator 13, and the combined multi-contingency (N-2) case with both outages applied simultaneously. Results are summarized in Table 12.

At 25 MVAr loading, SAO cut the line-outage loss from 12.1508 MW to 7.5774 MW (37.64%), the generator-outage loss from 13.6496 MW to 8.6843 MW (36.38%), and the combined multi-contingency loss from 13.9270 MW to 8.5120 MW (38.88%) — the algorithm still finds a workable solution with both outages applied at once. The three reductions cluster within about 2.5 percentage points of each other at this loading, with the multi-contingency case edging out the other two and the generator outage trailing slightly behind. That is a different picture from 0 MVAr, where the line outage clearly led (14.54%) and the generator outage lagged furthest behind (9.80%), with the multi-contingency case in between (10.16%) — the generator outage benefits least from optimization at both loadings, but the gap between scenarios narrows sharply as loading rises. We selected generator 13 for this analysis because it was ranked as the most severe generator outage based on SVSI in the contingency analysis of Section 2.2.3. The optimal control variable values for the 25 MVAr multi-contingency case are given in Table 13. Only T27-28 sits at its upper bound of 1.05 p.u.; the remaining twelve variables settle at interior values within the bounds defined in Table 1. The convergence curve for the 25 MVAr multi-contingency case is shown in Figure 6. SAO drops quickly to about 9.1354 MW within the first 31 iterations, then continues improving in smaller steps — 8.9163 MW by iteration 63 — before settling at its final loss of 8.5120 MW at iteration 114, considerably slower to settle than the no-outage case in Figure 5, where SAO reached its final solution within 32 iterations. Even so, the final loss under this combined outage remains higher than in the no-outage case. Across Cases 2 and 3, SAO consistently reduced transmission loss whether or not

Table 9. Transmission loss (MW) over ten trials for 50 moles at 150 iterations and 30 moles at 50 iterations

Trial	SAO (50, 150) MW	SAO (30, 50) MW
1	4.8330	4.8938
2	4.8656	4.8912
3	4.9067	4.8890
4	4.8503	4.8972
5	4.8807	4.8896
6	4.8674	4.8817
7	4.8538	4.8554
8	4.8591	4.8718
9	4.8469	4.8689
10	4.8530	4.8383
Average	4.8617	4.8777

Table 10. Transmission loss of ORPD without considering outage

Loading QL (MVAr)	Without outage pre (MW)	Without outage post (MW)	Loss reduction (%)
0	5.595	4.8606	13.1336
5	5.813	4.9630	14.6151
10	6.328	5.2158	17.5715
15	7.259	5.8139	19.9119
20	8.841	6.4110	27.4874
25	11.696	6.9554	40.5309

contingencies were present. All optimized control variables (Tables 8, 11, and 13) stayed within the bounds set in Table 1, so the equality and inequality constraints of the ORPD problem held throughout.

Table 11. Optimal control variables without contingency at bus 26 (50 moles, 150 iterations, 25 MVAr)

Variable (No. of moles)	Optimal value (Iteration = 50)
V1	0.9342 p.u.
V2	0.9000 p.u.
V5	0.9000 p.u.
V8	0.9066 p.u.
V11	0.9225 p.u.
V13	0.9000 p.u.
T6-9	0.9656 p.u.
T6-10	0.9500 p.u.
T4-12	1.0267 p.u.
T27-28	1.0500 p.u.
Qc3	18.5301 MVAr
Qc10	27.6125 MVAr
Qc24	2.5418 MVAr

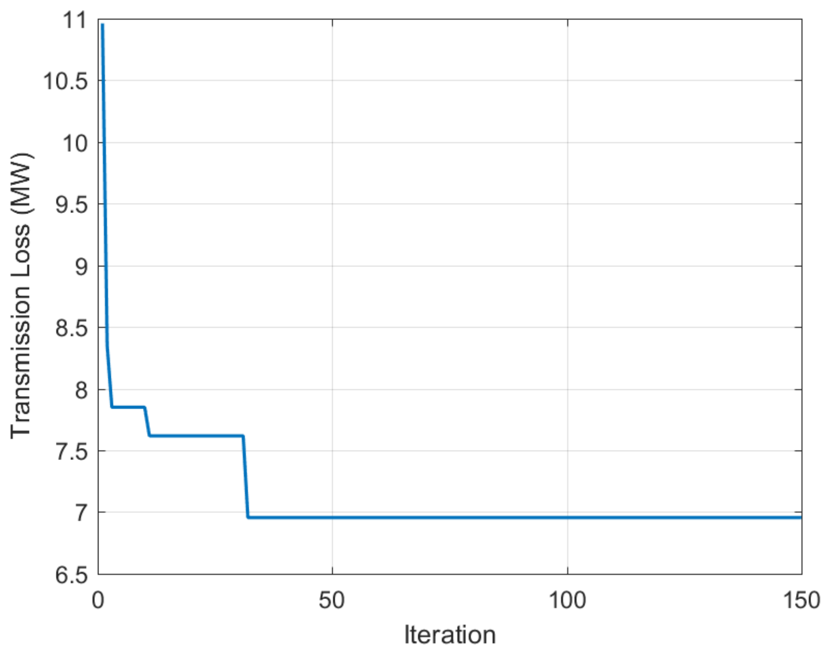

Figure 5. Convergence curve at bus 26 without contingency (number of moles = 50, iteration = 150)

Table 12. Transmission loss (MW) of SAO under contingency at bus 26 (50 moles, 150 iterations)

Loading QL (MVAr)	Analysis	Line outage at line 9	Generator outage at gen. 13	Multi-contingency (N-2)
0	Pre	6.1909	6.5706	7.0137
	Post	5.2906	5.9264	6.3008
5	Pre	6.4010	6.7800	7.2166
	Post	5.3773	6.0389	6.3674
10	Pre	6.9047	7.3104	7.7356
	Post	5.7077	6.3911	6.7535
15	Pre	7.8174	8.3051	8.7113
	Post	6.1565	6.9848	7.2474
20	Pre	9.3667	10.0738	10.4449
	Post	7.0644	7.7775	8.0206
25	Pre	12.1508	13.6496	13.9270
	Post	7.5774	8.6843	8.5120

3.5. Comparison with existing methods

To situate these results relative to the literature, Table 14 compares the SAO loss at 0 MVAr loading without contingency (4.8606 MW, from Table 10) against results reported for the same IEEE 30-bus system under comparable base-case conditions by invasive weed optimization (IWO) [32], the standard genetic algorithm (SGA), the harmony search algorithm (HSA), and particle swarm optimization (PSO), the latter three all reported in [33]. SAO achieves a lower loss than all four comparison methods under this base-case condition. A direct like-for-like comparison should still be read with caution, since these studies differ in software implementation, random seed, and stopping criteria; a full statistically validated benchmark against the same implementations under identical conditions is left as future work (Section 4).

Table 13. Optimal control variables for 25 MVAr multi-contingency at bus 26 (50 moles, 150 iterations)

Variable	Optimal value
V1	0.9775 p.u.
V2	0.9641 p.u.
V5	0.9976 p.u.
V8	0.9093 p.u.
V11	0.9093 p.u.
V13	1.0266 p.u.
T6-9	0.9600 p.u.
T6-10	0.9683 p.u.
T4-12	0.9728 p.u.
T27-28	1.0500 p.u.
Qc3	0.9532 MVAr
Qc10	-4.9445 MVAr
Qc24	17.2385 MVAr

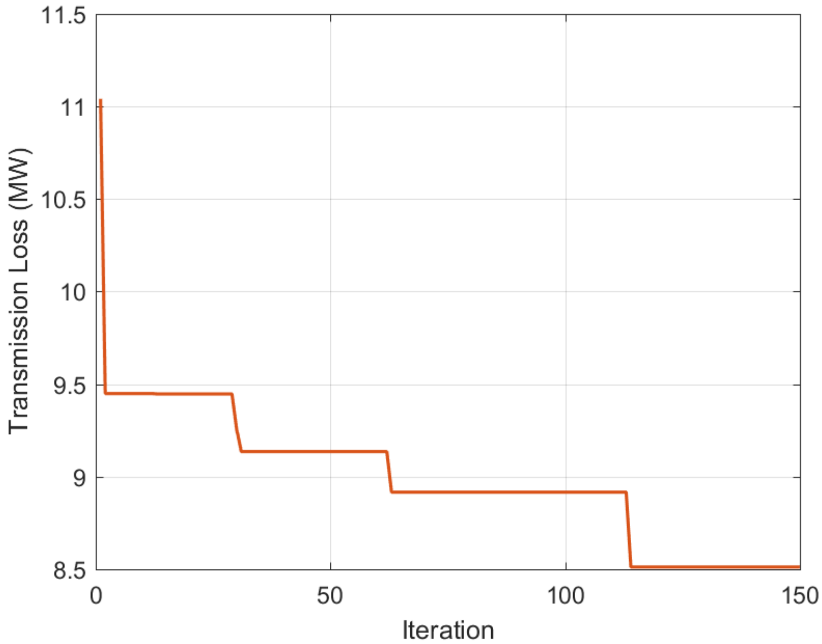

Figure 6. Convergence curve of 25 MVAr multi-contingency case at bus 26 (number of moles = 50, iteration = 150)

3.6. Stochastic validation and post-optimization feasibility diagnostics

To address the reviewer's request for repeated-run statistics and explicit feasibility evidence beyond control-variable settings, the fixed configuration (50 moles, 150 iterations) was run 30 independent times on the primary case (0 MVAr loading, no contingency - the same base case used in Section 3.2 to select this configuration). For every trial's best solution, the power flow was re-solved and checked against the case file's own bus voltage limits, generator reactive-power limits, and branch thermal ratings, in addition to load-flow convergence; Table 15 summarizes the results.

Full AC feasibility requires load-flow convergence together with zero violations of bus voltage, generator reactive-power, and branch thermal limits. This is stricter than, and separate from, the 13 control-variable bounds (Eqs. 8-10), which are enforced directly by the optimizer through boundary repair and were therefore satisfied in all 30 trials by construction. Every one of the 30 trials converged, and none exceeded any branch's thermal rating. However, none of

Table 14. Comparison of SAO transmission loss with existing methods on the IEEE 30-bus system at 0 MVAr loading without contingency

Algorithm	PLoss (MW)
SAO	4.8606
IWO [32]	4.9200
SGA [33]	6.5318
HSA [33]	5.1090
PSO [33]	5.8815

Table 15. Stochastic validation and post-optimization feasibility diagnostics over 30 independent trials (50 moles, 150 iterations, 0 MVAr, no contingency)

Metric	Value
Best loss (MW)	4.7736
Mean loss (MW)	4.8375
Median loss (MW)	4.8404
Standard deviation (MW)	0.0237
Worst loss (MW)	4.8704
Load-flow convergence rate	100% (30/30)
Full AC feasibility rate*	0% (0/30)
Mean bus voltage violations per run	15.1 buses
Mean / largest voltage violation magnitude	0.0485 / 0.0547 p.u.
Mean generator Q-limit violations per run	2.4 generators
Mean / largest Q-limit violation magnitude	9.97 / 16.26 MVAr
Branch thermal violations	0 (none in any run)
Function evaluations per run	30,000
Mean / median runtime per run	1257 s / 963 s

the 30 trials passed the full feasibility check: on average 15 of the system's 30 buses fell outside the case file's voltage limits (mean deviation 0.0485 p.u., largest 0.0547 p.u. across all trials), and on average 2 to 3 generators exceeded their reactive-power limit (mean 9.97 MVAr, largest 16.26 MVAr). These violation magnitudes are modest relative to the limits themselves, but they are systematic rather than occasional, which is consistent with the objective function (Eq. 3) being computed purely from the AC power-flow loss with no explicit penalty term for violating these particular limits (Section 2.1.3). Runtime per trial ranged from about 13 to 159 minutes (mean 1257 s, median 963 s) for a fixed 30,000 function evaluations, with the spread reflecting host-machine load during the runs rather than any difference in the amount of computation performed. A revised formulation that penalizes these remaining violations directly, with Tables 7-13 re-validated under that formulation, is identified as a direction for future work (Section 4).

Voltage-stability margin was assessed separately using the worst-line Static Voltage Stability Index (SVSI, Eq. 11): the unoptimized pre-ORPD baseline gave an SVSI_max of 0.1775 (on the line between buses 2 and 5), while five additional independent SAO runs of the same fixed configuration gave a mean post-ORPD SVSI_max of 0.1543 (best 0.1534, worst 0.1557), consistently on the same line. Since a lower SVSI indicates a larger margin before voltage collapse, the optimized dispatch improves the voltage-stability margin relative to the unoptimized base case, in addition to reducing transmission loss. As with the 30-trial validation above, none of these five runs satisfied the full feasibility check either, consistent with the systematic nature of that gap rather than being specific to any particular run.

4. Conclusions

This paper presented the application of the Smell Agent Optimization (SAO) algorithm to the optimal reactive power dispatch (ORPD) problem on the IEEE 30-bus reliability test system, with explicit consideration of multi-contingency conditions. Weak and secure buses were first identified using the Static Voltage Stability Index, and generator and line outages were ranked using the same index to select representative severe contingencies (generator 13 and line 9). A parametric study established 50 moles and 150 iterations as a consistent and effective SAO configuration. Using this configuration, SAO reduced transmission loss from 11.6957 MW to 6.9554 MW (40.5309%) at bus 26 under 25 MVAr loading without contingency, and from 13.9270 MW to 8.5120 MW under the combined line-and-generator multi-contingency case at the same loading, while all optimized control variables satisfied their equality and inequality constraints. SAO therefore holds up as an ORPD solver even when several contingencies hit the system at once. One caveat applies to the feasibility statement above: it refers specifically to the 13 control variables (Eqs. 8-10), which are enforced directly by the optimizer through boundary repair and are therefore always respected. A separate post-optimization check over 30 independent runs of the fixed configuration (Section 3.6) found that the generator reactive-power limit and the bus voltage limits defined in the case file were not always satisfied, although the violations were modest in magnitude, branch thermal ratings were never exceeded, and every load flow converged. This reflects the fact that the current objective function is computed purely from the AC power-flow loss, with no explicit penalty for violating these remaining limits elsewhere in the network. Incorporating such a penalty or repair mechanism and re-validating the results in Tables 7-13 under the revised formulation, is accordingly identified as a priority for future work, ahead of the other extensions discussed below. The SAO algorithm itself is one place to push further: its olfactory-coefficient tuning, adaptive parameters, or a more sophisticated search strategy could all sharpen the balance between exploration and exploitation. Contingency modelling is another. This study covered one line outage and one generator outage, so extending it to load fluctuations and network reconfiguration would give a fuller picture of how SAO holds up under stress. Beyond the specific test system considered here, the weak-bus identification and contingency-ranking framework used in this study is not tied to the IEEE 30-bus RTS and could, in principle, be applied to other transmission networks facing similar reliability requirements, offering utilities a practical route to prioritizing reactive-power dispatch under credible multi-contingency scenarios rather than a single worst case. Benchmarking SAO directly against other leading optimization techniques or commercial OPF software is also worth doing, to see how it compares on solution quality, convergence speed, and computational cost. By extending SAO to the multi-contingency ORPD problem, this study contributes a new data point on the algorithm's applicability beyond standard benchmark and single-outage settings, complementing existing PSO-based multi-contingency studies such as [13].

Acknowledgement
The authors gratefully acknowledge the Faculty of Electrical and Electronics Engineering Technology, Universiti Malaysia Pahang Al-Sultan Abdullah, for the facilities and support provided during this research.

Funding
This work was supported by Universiti Malaysia Pahang Al-Sultan Abdullah (UMPSA) under Grant (RDU200333).

Declaration of Competing Interest
The authors declare no conflicts of interest.

CRediT Authorship Contribution Statement
M. I. Salmizi (Writing - Original Draft; Formal Analysis; Visualisation; Data Curation)
N. R. H. Abdullah (Supervision; Writing - Review and Editing)
I. H. Shanono (Conceptualisation; Formal Analysis)
L. N. Muhammad (Writing - Review & Editing)

Availability of the Data and Materials
The datasets and MATLAB/MATPOWER simulation files generated and/or analysed during the current study are available from the corresponding author on reasonable request.

Ethical Declaration
This study did not involve human participants, animal subjects, or personal data. It is a computational simulation study of an IEEE standard test system, and ethical approval was therefore not required.

Generative Artificial Intelligence Declarations
Artificial intelligence tools were used to assist in drafting sections of the manuscript and summarizing literature. The authors reviewed and verified all AI-generated content to ensure accuracy and originality. Final interpretations and conclusions are the responsibility of the authors.

REFERENCES
[1] A. Khamees, N. Badra, and A. Y. Abdelaziz, "Optimal Power Flow Methods: A Comprehensive Survey," *Int. Electr. Eng. J.*, vol. 7, no. 4, pp. 2228–2239, 2016.
[2] W. Lai, Q. Song, X. Zheng, and H. Chen, "The study of optimal reactive power dispatch in power systems based on further improved membrane search algorithm," *Appl. Energy*, vol. 377, p. 124433, Dec. 2024, doi: 10.1016/j.apenergy.2024.124433.
[3] V. Loriya and V. Patel, "A Review on Optimal Reactive Power Dispatch," *Int. J. Innov. Res. Electr. Electron. Instrum. Control Eng.*, vol. 4, no. 1, pp. 83–87, Jan. 2016, doi: 10.17148/ijireeice.2016.4120.
[4] B. Jiang, Q. Wang, S. Wu, Y. Wang, and G. Lu, "Advancements and Future Directions in the Application of Machine Learning to AC Optimal Power Flow: A Critical Review," *Energies*, vol. 17, no. 6, p. 1381, Mar. 2024, doi: 10.3390/en17061381.
[5] D. Chauhan, A. Yadav, and S.-B. Cho, "AEFA-FDB: A score-based artificial electric field algorithm for optimal reactive power dispatch problem with renewable and load demand uncertainties," *Appl. Soft Comput.*, vol. 180, p. 113292, Feb. 2025, doi: 10.1016/j.asoc.2025.113292.
[6] R. Roy, T. Das, and K. K. Mandal, "Optimal reactive power dispatch using a novel optimization algorithm," *J. Electr. Syst. Inf. Technol.*, vol. 8, no. 1, p. 11, Dec. 2021, doi: 10.1186/s43067-021-00041-y.

[7] M. S. Saddique, A. R. Bhatti, S. S. Haroon, M. K. Liaquat, S. Sattar, and S. S. S. Gardezi, "Solution to optimal reactive power dispatch in transmission system using meta-heuristic techniques — Status and technological review," *Electr. Power Syst. Res.*, vol. 178, p. 106031, Jan. 2020, doi: 10.1016/j.epsr.2019.106031.
[8] J. Jithendranath and B. Y. Babu, "Solving ORPD problem with modal analysis by differential evolution," in *Proc. 2nd Int. Conf. Electr. Energy Syst. (ICEES)*, 2014, pp. 51–55, doi: 10.1109/ICEES.2014.6924140.
[9] P. Singh, P. Purey, L. S. Titare, and S. C. Choube, "Optimal reactive power dispatch for enhancement of static voltage stability using jaya algorithm," in *Proc. Int. Conf. Intell. Circuits Syst. (ICICIC)*, 2018, pp. 1–5, doi: 10.1109/ICOMICON.2017.8279044.
[10] M. G. Gafar, R. A. El-Sehiemy, and H. M. Hasanien, "A novel hybrid fuzzy-Jaya optimization algorithm for efficient ORPD solution," *IEEE Access*, vol. 7, pp. 182078–182088, 2019, doi: 10.1109/ACCESS.2019.2955683.
[11] H. Modha and V. Patel, "Minimization of Active Power Loss for Optimum Reactive Power Dispatch using PSO," in *Proc. IEEE Int. Conf. Emerg. Trends Ind. 4.0 (ETI 4.0)*, 2021, pp. 1–5, doi: 10.1109/ETI4.051663.2021.9619313.
[12] F. R. Cabezas Soldevilla and F. Alfredo Cabezas Huerta, "Minimization of Losses in Power Systems by Reactive Power Dispatch using Particle Swarm Optimization," in *Proc. 54th Int. Univ. Power Eng. Conf. (UPEC)*, 2019, pp. 1–6, doi: 10.1109/UPEC.2019.8893527.
[13] N. R. H. Abdullah, M. Mustafa, R. Samad, D. Pebrianti, and L. N. Muhammad, "PSO based optimal reactive power dispatch (ORPD) considering multi-contingencies," *J. Telecommun. Electron. Comput. Eng.*, vol. 10, no. 1–3, pp. 41–44, 2018.
[14] R. Ng Shin Mei, M. H. Sulaiman, Z. Mustaffa, and H. Daniyal, "Optimal reactive power dispatch solution by loss minimization using moth-flame optimization technique," *Appl. Soft Comput.*, vol. 59, pp. 210–222, Oct. 2017, doi: 10.1016/j.asoc.2017.05.057.
[15] S. Mugemanyi, Z. Qu, F. X. Rugema, Y. Dong, C. Bananeza, and L. Wang, "Optimal Reactive Power Dispatch Using Chaotic Bat Algorithm," *IEEE Access*, vol. 8, pp. 65830–65867, 2020, doi: 10.1109/ACCESS.2020.2982988.
[16] M. Lakshmi and A. Ramesh Kumar, "Optimal reactive power dispatch using crow search algorithm," *Int. J. Electr. Comput. Eng.*, vol. 8, no. 3, pp. 1423–1431, Jun. 2018, doi: 10.11591/ijece.v8i3.pp1423-1431.
[17] A. Askarzadeh, "A novel metaheuristic method for solving constrained engineering optimization problems: Crow search algorithm," *Comput. Struct.*, vol. 169, pp. 1–12, Jun. 2016, doi: 10.1016/j.compstruc.2016.03.001.
[18] T. Das and R. Roy, "A novel algorithm for the Optimal Reactive Power Dispatch," in *Proc. 20th Natl. Power Syst. Conf. (NPSC)*, 2018, pp. 1–6, doi: 10.1109/NPSC.2018.8771809.
[19] S. Salhi, D. Naimi, A. Salhi, S. Abujarad, and A. Necira, "A novel hybrid approach based artificial bee colony and salp swarm algorithms for solving ORPD problem," *Indones. J. Electr. Eng. Comput. Sci.*, vol. 23, no. 3, pp. 1825–1837, Sep. 2021, doi: 10.11591/ijeecs.v23.i3.pp1825-1837.
[20] C. R. Chen, C. Y. Lee, Y. F. Hsu, and H. W. Chao, "Optimal reactive power dispatch of power systems using a modified genetic algorithm," in *Proc. Int. Conf. Power Syst. Technol. (POWERCON)*, 2004, vol. 2, pp. 1266–1269, doi: 10.1109/icpst.2004.1460196.
[21] Y. M. Zhang, C. R. Chen, and C. Y. Lee, "Solution of the optimal reactive power dispatch for power systems by using novel charged system search algorithm," in *Proc. 7th Int. Symp. Next-Gener. Electron. (ISNE)*, 2018, pp. 1–4, doi: 10.1109/ISNE.2018.8394748.
[22] M. Ebeed, A. Alhejji, S. Kamel, and F. Jurado, "Solving the optimal reactive power dispatch using marine predators algorithm considering the uncertainties in load and wind-solar generation systems," *Energies*, vol. 13, no. 17, p. 4316, Aug. 2020, doi: 10.3390/en13174316.
[23] M. Ebeed, S. Ali, A. M. Kassem, M. Hashem, S. Kamel, and F. Jurado, "Solving stochastic optimal reactive power dispatch using an Adaptive Beluga Whale optimization considering uncertainties of renewable energy resources and the load growth," *Ain Shams Eng. J.*, vol. 15, no. 7, p. 102762, Jul. 2024, doi: 10.1016/j.asej.2024.102762.
[24] R. Jamal, J. Zhang, B. Men, N. H. Khan, M. Ebeed, and S. Kamel, "Solution to the deterministic and stochastic optimal reactive power dispatch by integration of solar, wind-hydro powers using modified artificial hummingbird algorithm," *Energy Rep.*, vol. 9, pp. 4157–4173, Dec. 2023, doi: 10.1016/j.egyr.2023.03.036.
[25] M. Ebeed, A. Ali, M. I. Mosaad, and S. Kamel, "An improved lightning attachment procedure optimizer for optimal reactive power dispatch with uncertainty in renewable energy resources," *IEEE Access*, vol. 8, pp. 168721–168731, 2020, doi: 10.1109/ACCESS.2020.3022846.
[26] A. T. Salawudeen, M. B. Mu'azu, A. Yusuf, and E. A. Adedokun, "From smell phenomenon to smell agent optimization (SAO): A feasibility study," in *Proc. Int. Conf. Green Energy Technol. (ICGET)*, May 2018, pp. 79–85.
[27] S. S. Vinod Chandra, "Smell Detection Agent Based Optimization Algorithm," *J. Inst. Eng. India Ser. B*, vol. 97, no. 3, pp. 431–436, Sep. 2016, doi: 10.1007/s40031-014-0182-0.
[28] A. T. Salawudeen, M. B. Mu'azu, Y. A. Sha'aban, and A. E. Adedokun, "A Novel Smell Agent Optimization (SAO): An extensive CEC study and engineering application," *Knowl.-Based Syst.*, vol. 232, p. 107486, Nov. 2021, doi: 10.1016/j.knosys.2021.107486.
[29] H. Saadat, *Power System Analysis*. New York, NY, USA: McGraw-Hill, 1999.
[30] L. Qi, "AC system stability analysis and assessment for shipboard power systems," Ph.D. dissertation, Dept. Electr. Eng., Texas A&M Univ., College Station, TX, USA, 2004.
[31] N. Nazir, N. Gupta, and R. Farishta, "Contingency Analysis in Power System Studies: A Critical Review," in *Proc. 4th Int. Conf. Mach. Learn., Adv. Comput., Renewable Energy Commun. (MARC 2023)* (Lecture Notes in Electrical Engineering, vol. 1231), Singapore: Springer, 2024, pp. 85–97, doi: 10.1007/978-981-97-5227-0_9.

[32] M. Ghasemi, S. Ghavidel, M. M. Ghanbarian, and A. Habibi, "A new hybrid algorithm for optimal reactive power dispatch problem with discrete and continuous control variables," *Appl. Soft Comput.*, vol. 22, pp. 126–140, Sep. 2014, doi: 10.1016/j.asoc.2014.04.036.
[33] A. H. Khazali and M. Kalantar, "Optimal reactive power dispatch based on harmony search algorithm," *Int. J. Electr. Power Energy Syst.*, vol. 33, no. 3, pp. 683–692, Mar. 2011, doi: 10.1016/j.ijepes.2010.11.007.